Journal of Volcanology and Geothermal Research, 16 (1983) 189—203
Elsevier Science Publishers B.V., Amsterdam — Printed in The Netherlands

CONDUCTION MODELS OF THE TEMPERATURE DISTRIBUTION IN THE EAST RIFT ZONE OF KILAUEA VOLCANO

ALBERT J. RUDMAN and DAVID EPP

Department of Geology, Indiana University, Bloomington, IN 47405 (U.S.A.)
Hawaii Institute of Geophysics, University of Hawaii, Honolulu, HI 96822 (U.S.A.)

(Received November 13, 1981; revised and accepted July 20, 1982)

ABSTRACT

Rudman, A.J. and Epp, D., 1983. Conduction models of the temperature distribution in the East Rift Zone of Kilauea volcano. J. Volcanol. Geotherm. Res., 16: 189—203.

Temperature variations in the 1966-meter Hawaii Geothermal Project well HGP-A are simulated by model studies using a finite element code for conductive heat flow. Three models were generated: a constant temperature source from a vertical dike; a constant heat-generating magma chamber; and a transient heat source from a tapered vertical dike. Fair correlation is obtained between the HGP-A well temperature and the tapered dike 125 years after it is injected with an initial (transient) 1200° C temperature. Results provide background information from which to evaluate the importance of water convection in maintaining the temperature distribution in the East Rift Zone.

INTRODUCTION

The Hawaii Geothermal Project well HGP-A was drilled to a depth of 1966 m on the lower East Rift Zone (ERZ) of Kilauea volcano on the island of Hawaii (Fig. 1). Since its completion there has been considerable interest in the thermal structure of the ERZ, as demonstrated by the generation of a number of thermal models by Cheng (see Cheng and Lau, 1978, for a summary). Cheng's models emphasize the effects of water convection under various boundary conditions in a liquid-dominated volcanic island regime. His models can degenerate to conduction models (for small Rayleigh numbers); thus some of the conduction results presented in this study could also be derived from Cheng's work given the proper boundary conditions and input parameters.

Since the permeability of the ERZ is poorly known, it is difficult to evaluate the importance of water convection in controlling the temperature distribution. Thus, we have chosen to start with a basic approach: given what is known about the structure, dynamics, and physical properties of the rift

---

Hawaii Institute of Geophysics Contribution No. 1326.

zone, conduction models are generated to match the vertical temperature distribution measured in HGP-A. Such models provide background data to properly evaluate the importance of water convection within the ERZ and, thereby, adapt the generalized results of Cheng and co-workers to the geothermal reservoir of Puna.

GEOLOGY

Kilauea magma comes from depths of at least 60 km in the mantle (Eaton and Murata, 1960). Studies of ground deformation indicate that the upper summit of Kilauea expands as magma rises and inflates a reservoir system located 2—5 km below the summit (Eaton, 1962; Fiske and Kinoshita, 1969; Koyanagi et al., 1976). Sometimes magma from this reservoir moves upward to produce a summit eruption; at other times magma from the summit reservoir moves laterally into the ERZ, accompanied by a deflation of the summit reservoir. Epp et al. (in press) have shown that the amount of magma leaving the summit reservoir is inversely related to the elevation of the eruption on the ERZ.

Swanson (1972) calculated that magma is supplied to Mauna Loa and Kilauea from the mantle at a rate of about 9×10^6 m^3/month. Dzurisin et al. (1980) have obtained similar values. Swanson suggested that during inactivity at Mauna Loa, magma is pumped into Kilauea's plumbing system and that much of it might pass through the rift zones to be extruded on the sea floor. Eruptions have occurred in the Puna area in about 1750 and 1790, and in 1840, 1955, and 1960. In 1884 a submarine eruption occurred a few kilometers offshore, and in 1924 a large volume of magma moved eastward through the ERZ (Macdonald, 1977). In addition, there have been injections (without eruptions) into the ERZ that may have transported magma into the lower ERZ (see Klein, 1982). Thus there has been a magmatic event in this section of the ERZ at least every 32 years. Some, if not all, of these magmatic events renew the heat source for HGP-A.

The location of eruptive fissures along the ERZ (Fig. 1) indicate that the ERZ is about 3 km wide at the surface; it may be wider at depth. The line of eruptive vents, pit craters, and fissures that follow the axis of the ERZ is offset in the vicinity of HGP-A. The contact between Mauna Loa and the original sea floor is located under Kilauea at approximately the location of the offset in the ERZ (see fig. 3 in Epp et al., in press). Thus, to the west of the offset, the rift zone is buttressed by Mauna Loa and expansion of the rift zone results in a southward displacement of the south flank of Kilauea. East of the offset, the rift zone is not buttressed by Mauna Loa and, consequently, the rift zone can expand both to the north and to the south (see also Suyenaga and Furumoto, 1978; Zablocki and Koyanagi, 1979).

Rift zone dike complexes are exposed by erosion in older Hawaiian volcanoes. Most dikes are less than 1.5 m thick, although some may be as thick as 15 m (Macdonald, 1977). The dikes trend in various directions, but most

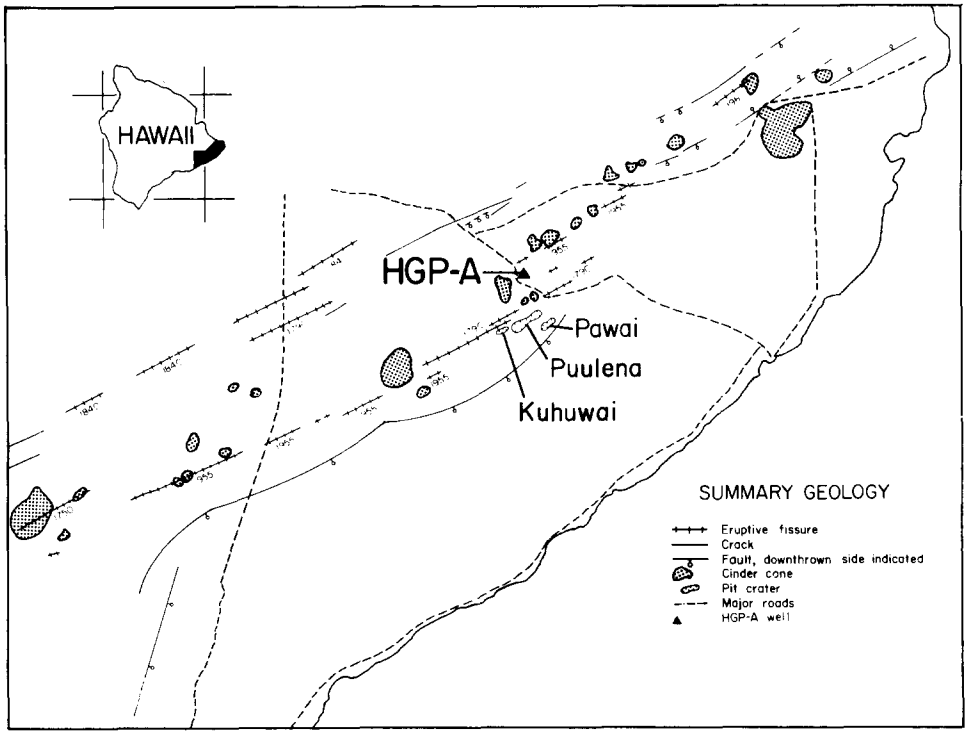

Fig. 1. Index map of Hawaii showing location of HGP-A well, East Rift Zone and volcanic centers.

dikes trend within 20° of the trend of the rift zone, and more than 85% of the exposed dikes dip less than 10° from vertical (Macdonald, 1977). Exposed dikes, commonly separated by wedges of older lava flows, comprise 25—50% of the total rock in the rift zone.

Wright and Fiske (1971) have shown that magma is supplied to the summit reservoir complex in batches that differ slightly in composition. They suggest that the appearance of a given summit magma type in an ERZ eruption, before it appears in a summit eruption, shows that the summit reservoir complex is crudely zoned in vertical section with the deeper parts containing younger magma. Conduits within the ERZ seem to be largely isolated from one another, with the results that magma can be stored and fractionated to various degrees in different conduits. During late prehistoric times, pockets of magma differentiated within the rift zone.

Macdonald (1977) pointed out that the pit craters Kahuwai, Pawai, and Puulena, located south of HGP-A, were formed by collapse, probably above stocks that emptied or cooled and contracted (see Macdonald and Eaton, 1964). The largest of these pit craters, Puulena, is about 250 m wide and 700 m long, and its long axis parallels the rift zone. The analysis of Blevins (1981) has shown that the size of pit craters is most strongly controlled by the

depth to an underlying void, and that its diameter may be several times the diameter of the void. These craters are located just to the west (upslope) of the offset in the ERZ. Deep structure associated with this offset may constrict the flow of magma along the ERZ; thus the offset is an obvious place for impounding and storage of magma within the rift zone. Vents of the 1955 eruption occur both up rift and down rift from HGP-A (Macdonald and Eaton, 1964). Using the data provided by Macdonald and Eaton (1964, table 1) and Wright and Fiske (1971, table 5) we calculate that about 76 $\times$ 10^6 m^3 of magma was stored in this section of the ERZ prior to the 1955 eruption.

These data indicate that magma is transported and stored (at least at shallow levels) in the ERZ in a series of 1—15-m-wide dikes, and that magma is injected into the lower ERZ at least every 32 years. Much less certain is the existence of larger conduits lower in the ERZ. Epp et al. (in press) suggested that aseismic leakage of magma from the summit reservoir into the ERZ, together with the larger seismic injections, might raise the temperature of relatively large areas to melting, forming large conduits at depth. Since such conduits have not been exposed by erosion in older volcanoes, their existence is speculative.

Lithologic and physical parameters to constrain the thermal models were obtained from studies of the HGP-A well samples (Palmiter, 1976). For example, although there is high porosity and permeability in the nearby surficial materials, lithologies in HGP-A show that pillow basalts of low porosity are dominant below 520 m. Whatever permeability is available in the lower part of the well, therefore, is presumed to be associated with fractures, many of which are locally filled with secondary minerals (Palmiter, 1976; Stone, 1977).

TEMPERATURES IN HGP-A

Drilling of HGP-A was completed on April 28, 1976. An equilibrium temperature was not measured in HGP-A; the well was flashed before the drilling disturbance was dissipated. However, before the mud was pumped out, temperatures in the well were measured at 15, 75, 97, 145, and 193 hours, and at 13, 21, and 22 days after circulation of the drilling mud stopped. These temperature data are shown in Fig. 2. Between 305 m and 914 m temperatures were measured only at 15 and 75 hours, and indicate that this part of the well was cooling slowly. Our estimate of the undisturbed temperature gradient to 914 m (Fig. 3) is somewhat lower than that observed in the 75-hour log for those depths. Eight temperature logs were obtained between 1158 m and 1340 m. Because the mud was settling into the bottom of the well, the level to which the Kuster gauge could penetrate decreased with time. Consequently, repeated temperature measurements are not available at depths below 1372 m.

The observed repeated borehole temperature measurements were extrapolated to an equilibrium temperature following the method of Bullard (1947)

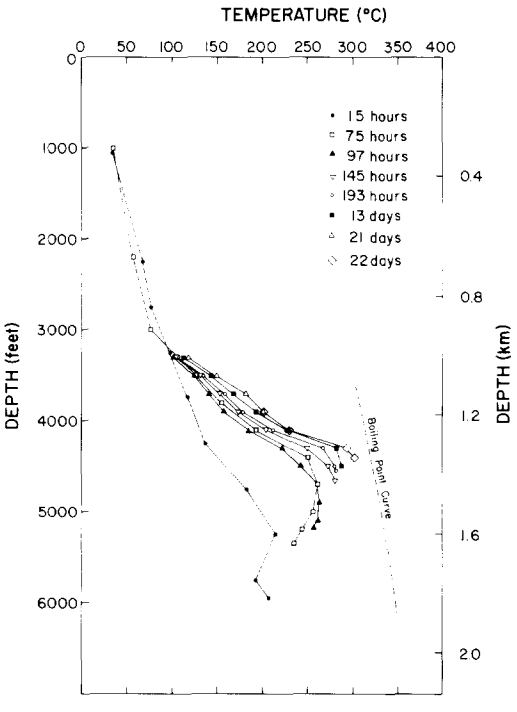

Fig. 2. Temperatures measured in HGP-A and an approximated boiling point of water curve.

and Lachenbruch and Brewer (1959). This is done graphically by plotting the measured temperatures against $\ln(1+s/t_m)$, where s is the time elapsed from the time the drill reached a given depth to the time the drilling ceased, and t_m is the time from the end of the drilling to the temperature measurement at the same depth. The equilibrium temperature is obtained by extrapolating the plot to $\ln(1+s/t_m) = 0$. The dots in Fig. 3 show the extrapolated temperatures between 914 and 1372 m.

The available data indicate that the temperature gradient is decreasing below about 1340 m, and that the temperature at 1372 m is very close to the boiling point of water at that depth (Fig. 2). In a permeable water-filled rift zone, water can convect through the rift zone. If the temperature rises above the boiling point, the water will flash to steam which will be convected away until the temperature falls below the boiling point. Thus, in water-filled parts of the ERZ the steady-state temperature is unlikely to rise above the boiling point of water at any given depth. Since the temperature at 1372 m is close to the boiling point, and the temperature gradient seems to be decreasing below this depth, we assume that the boiling point curve approximates the undisturbed temperature below 1372 m.

An undisturbed water level was not measured in HGP-A. The water wells near HGP-A, however, have a water level within about one meter of sea level,

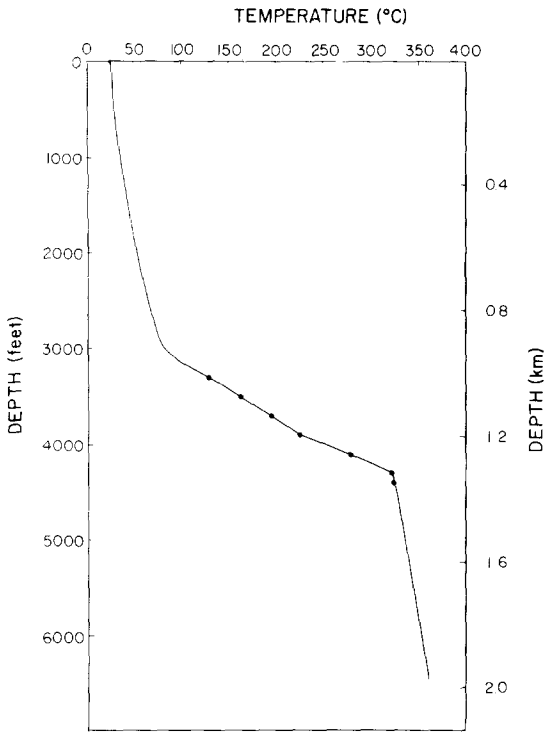

Fig. 3. Estimated undisturbed temperature distribution in the vicinity of HGP-A.

which is approximately 187 m below ground level at HGP-A. We therefore assume that hydrostatic pressures prevail below 187 m and have calculated the boiling point curve shown in Fig. 2 on that basis. This curve approximates the undisturbed temperature gradient below 1340 m (Fig. 3). We also assume a surface temperature of 25°C. A temperature profile similar to that shown in Fig. 3 was estimated by Helsley (1977).

FINITE-ELEMENT COMPUTATION

A two-dimensional finite-element code developed by Lee et al. (1980) was used in this study to calculate transient and steady-state models. Lee gives a complete theoretical development and his approach is only outlined in this report.

Heat conduction is described by the equation:

$$\nabla(K\nabla T) + Q = \alpha \frac{\partial T}{\partial t} \tag{1}$$

where T = temperature, t = time, K = thermal conductivity, Q = heat production per unit volume per unit time, and $\alpha = \partial c$ = heat capacity, ρ = density, c specific heat at constant pressure. Two types of boundary conditions may be specified: (1) constant temperature at the upper and lower boundaries; or

(2) normal heat flux at the lower boundary. For the transient problem, initial conditions must also be specified.

A unique solution of eq. 1 can be obtained by the finite-element method based on the calculus of variations (Zienkiewicz, 1977). Equation 1 is at any instant equivalent to the minimization of the functional $X(u)$:

$$X(u) = \int_V [\frac{K}{2} \nabla T \cdot \nabla T - (Q - \alpha \frac{\partial T}{\partial t}) T] dV + \int_S q T dS \quad (2)$$

where q is either heat input (−) or output (+), S is the surface on which the boundary conditions are to be satisfied and $u(x,y,z)$ is a function we seek to minimize the integral. The region under consideration is separated into triangular finite elements inter-connected at nodal points. Specific material properties such as heat generation, conductivity, and diffusivity are assigned to each element with temperatures within and on the boundary expressed in terms of temperatures at nodes associated with the element concerned. At the boundary between materials, the tangential derivative and the normal component of the heat flux are continuous. Minimization of the functional X yields a first-order differential equation whose solution depends on linear interpolation of temperature. Once the temperature is computed, the directional heat flux can be calculated in terms of nodal temperatures.

Geometry of the area modeled is specified by the number of columns and rows of elements in the region along with the topographic (surface) coordinates in kilometers. Conductivity, diffusivity, and heat production are specified for the entire region. If there is an anomalous zone within the region, coordinates of the zone are specified along with its material properties. The user stipulates the boundary and initial regional temperature conditions, and the time intervals if a transient problem is being considered.

An intrusive body can be characterized by assigning various initial temperatures to nodes that define the body area. Lee's algorithm provided input for a constant temperature throughout the region, but did not include a provision to input various temperatures at each node. The code was modified in this study to permit this flexibility.

Normal output consists of both graphic and numerical tabulations of vertical and horizontal heat flow, as well as a plot of isotherms (contours) superposed on a geometric sketch of the model. For this study, only the isotherms are reproduced as figures.

CONDUCTION MODELS

The purpose of this study is to provide baseline conductive models from which to compare the relative importance of convection of water in the ERZ. While the geology and dynamics of the ERZ indicate that there are repeated injections into 1—15-m-wide dikes, we have chosen in this study to approximate a wider dike complex with injections at greater time intervals.

The physical properties of Hawaiian basalts are strongly dependent on the porosity of the basalt, and on the amount of filling of the pores by alteration products and/or water. Because porosity and pore filling are highly variable in HGP-A samples, we have used average values for thermal conductivity and diffusivity. Thermal diffusivities of HGP-A samples were measured by Manghnani et al. (1976, 1977), and thermal conductivities of Hawaiian basalts were measured by Robertson and Peck (1974). Regional conductivity of the country rock was set at 2.5 W/m °K and diffusivity at 1.0×10^{-6} m^2/s. Within a magma chamber, conductivity and diffusivity were estimated at 1.1 W/m °K and 0.6×10^{-6} m^2/s. Boundary-condition temperatures generally were set at 1200° to approximate magma at relatively shallow depths. Surface temperatures of 25°C approximated ambient temperatures in the area.

The observed temperatures are modelled in three ways: (I) a constant temperature source simulating a vertical dike connected to a magma chamber, (II) a steady heat generation simulating a small magma chamber; and (III) a transient heat source simulating a tapered dike. Although models I and II are often used to simulate dike intrusions (e.g., Horai, 1974), the isotherms generated for these models did not closely resemble the observed variations in the HGP-A. region. Model III, however, did successfully match the temperatures. Results are summarized in the following sections.

(I) Constant temperature source from an intrusive dike

Model I simulates a thin vertical dike intruded into a region 0.25 km wide and 3.0 km deep (Fig. 4). A constant 1200°C temperature is applied at time zero along the bottom boundary of the region to simulate a chamber at depth. The upper surface is fixed at 25°C. Regional conductivity is 2.5 W/m °K and diffusivity is 1.0×10^{-6} m^2/s. Transient solutions were computed at time intervals less than $x^2/2D$ seconds, where D is the diffusivity and x is the smallest linear dimension of the elements; for Model I this is 1.5 years. Only slight differences were observed between computer runs based on a 1.5-year and a 30-year time interval. In the interest of computing efficiency, and to match the approximately 30-year sequence of magmatic intrusions, isotherms were plotted at 30 and 60 years after the dike is intruded (Fig. 4).

The vertical dike simulated by Model I is considered to be connected to a magmatic source at 3 km depth. Temperatures for numerous models of varying dike thicknesses and depths of burial were calculated and compared with the observed temperatures in the well. For Model I, the best fit to the observed data is a dike approximately 25 m wide with its top 0.9 km from the surface. The large horizontal exaggeration in Fig. 4 makes the dike wall appear inclined, but it is essentially vertical.

Figure 4A shows the isotherms 30 years after the 1200°C temperature is applied, and Fig. 4B demonstrates the outward heat flow after 60 years; the isotherms are systematically displaced with time away from the dike. Use of

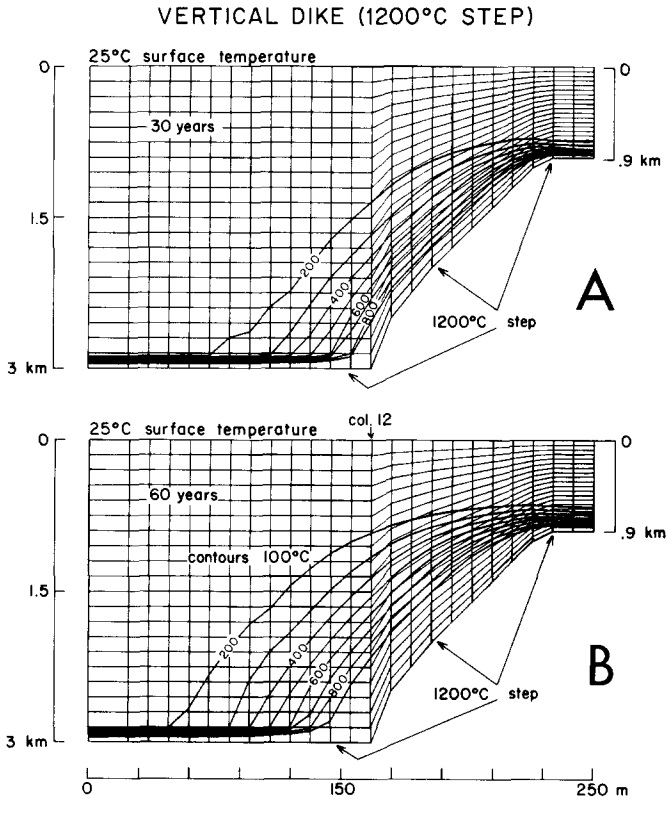

Fig. 4. Isotherms at 30 years (A) and 60 years (B) after a constant 1200°C temperature is applied. The indentation along the bottom of the figure simulates the intruded dike.

a higher diffusivity (7×10^{-6} m^2/s instead of 1×10^{-6} m^2/s) displaced the isotherms away from the dike but did not improve the comparison with observed temperatures in the well. The vertical variation of temperature adjacent to the dike (col. 12 in Fig. 4B) is plotted in Fig. 5 and compared to the HGP-A temperature profile.

The best fit between model and observed temperature occurs after 60 years. Although the model fits the observed data in the interval from 0.9 to 1.3 km, it does not adequately match elsewhere, especially below 1.3 km. If we assume our extrapolation of temperatures below 1.3 km to be approximately correct, the model temperature do not adequately simulate the conditions near HGP-A. Model I is, therefore, not considered acceptable.

(II) Steady heat generation from a magma chamber

Model II simulates a small magma chamber within an area 6.0 km wide and 3.0 km deep (Fig. 6). Regional conductivity and diffusivity are again 2.5 W/m °K and 1.0×10^{-6} m^2/s, respectively. A surface temperature of 25°C is

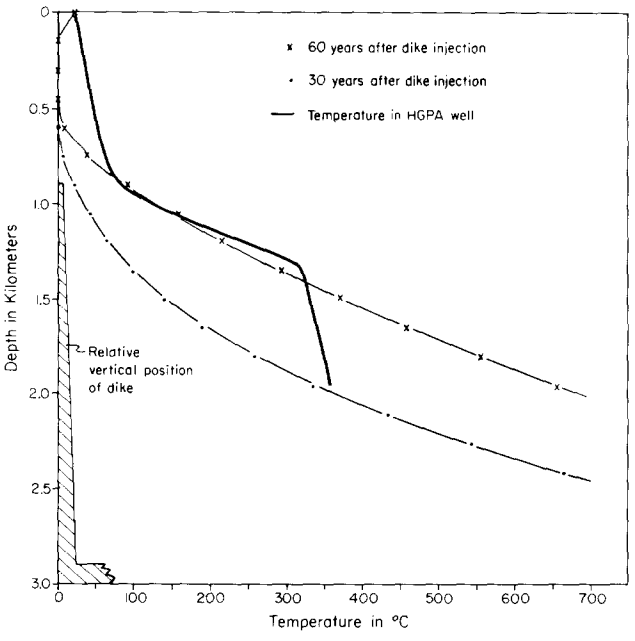

Fig. 5. Observed temperatures in the HGP-A well and model temperatures of a vertical dike with constant temperature source. Calculations were made at a point adjacent to the (model) dike wall. Because of the symmetry conditions, only half of the area needs to be displayed.

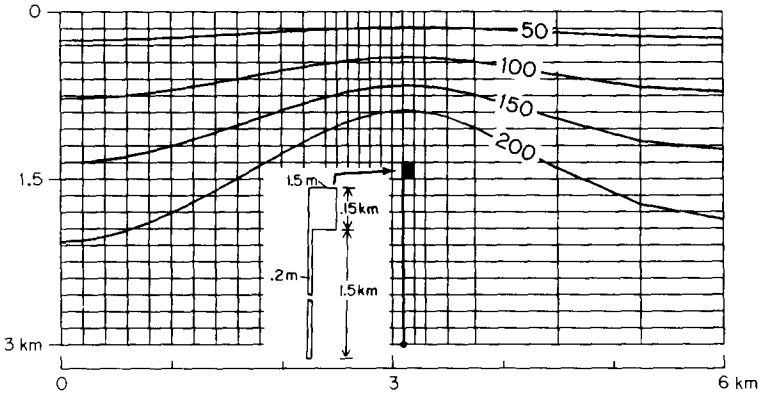

Fig. 6. Isotherms associated with a model of a magma chamber fed by a thin vertical dike. The chamber and dike are a constant generating heat source.

imposed as one boundary condition. A heat flux of 60 mW/m^2 is assumed for the lower boundary. This typical geothermal flux imposes a reasonable geothermal gradient of 24° C/km used as an initial condition for the temperature distribution. Numerous models were tested before selecting the optimum model: a small, constant generating heat source of 3.2×10^{-6} W/m^3 located 1.3 km below the surface.

This two-dimensional model simulates a magma chamber with rectangular cross section 1.50 X 150 m; conductivity and diffusivity are 1.1 W/m °K and 0.6 X 10^{-6} m^2/s, respectively. The chamber is connected to a long thin (0.2 m) vertical dike with the same heat generation, conductivity, and diffusivity as the chamber. A slow movement of magma along the dike, such as that accompanying aseismic deflation of the summit reservoir (Epp et al., in press), might maintain a constant heat source in such a chamber.

A plot of the steady-state isotherms normalized to 60 mW/m (Fig. 6) shows the expected maximum over the magma chamber. The observed HGP-A data and the steady state model temperatures are plotted at distances of 100, 500 and 1500 m from the source (Fig. 7A). The constant heat source, in the steady state, yields a slowly changing temperature with depth. The observed temperatures, however, show rapid change in gradient with depth and do not compare favorably with the model data.

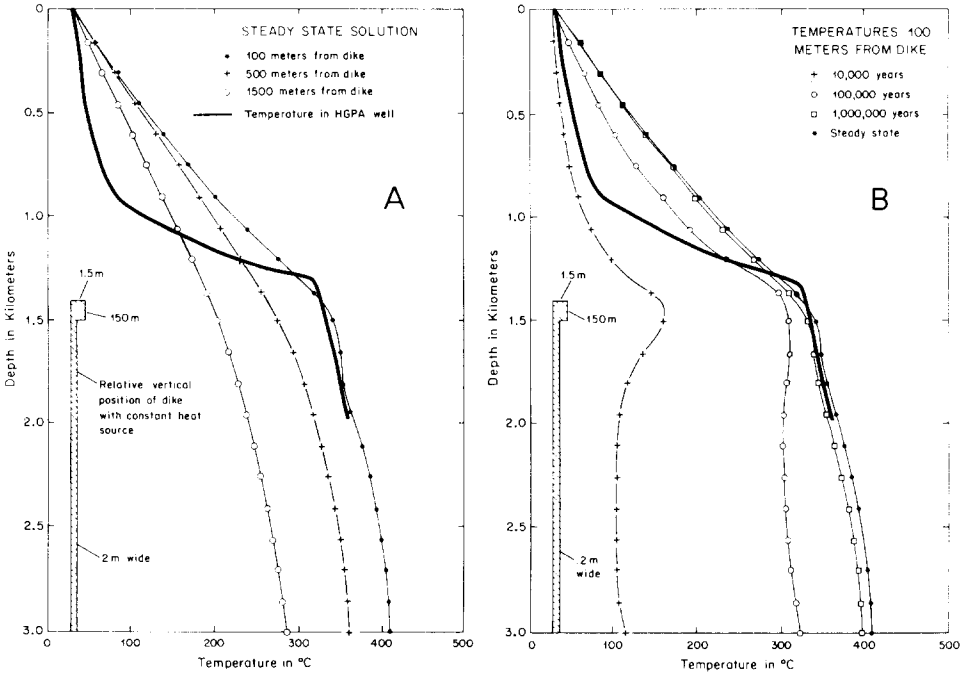

Fig. 7. Temperatures observed in the HGP-A well and (A) temperatures at 100, 500, and 1500 m from a model of a magma chamber with a thin vertical dike and (B) temperatures 100 m from the model at 10,000, 100,000, and 1,000,000 years and at steady state.

The observed HGP-A temperatures and the model data at 100 m from the source are plotted at 10,000, 100,000 and 1,000,000 years, and at steady-state times (Fig. 7B). Chambers of various sizes were modelled at various depths, but no reasonable fit was found and the model is rejected. Nevertheless, the thin vertical dike may not be entirely unreasonable; the tempera-

tures associated with the dike do match the observed temperatures below 1.3 km.

(III) A transient heat source from a tapered dike

Model III is a tapered dike intruded into an area 1.0 km wide by 3.0 km deep (Fig. 8). Regional conductivity is 2.5 W/m °K and diffusivity is 1.0×10^{-6} m^2/s. Surface temperature is 25°C and a heat flux of 100 mW/m^2 is fixed for the lower surface (the boundary condition of 100 W/m^2 yields a gradient of 40°C/km necessary to match observed and model temperatures). Transient temperatures were computed in time steps of one year.

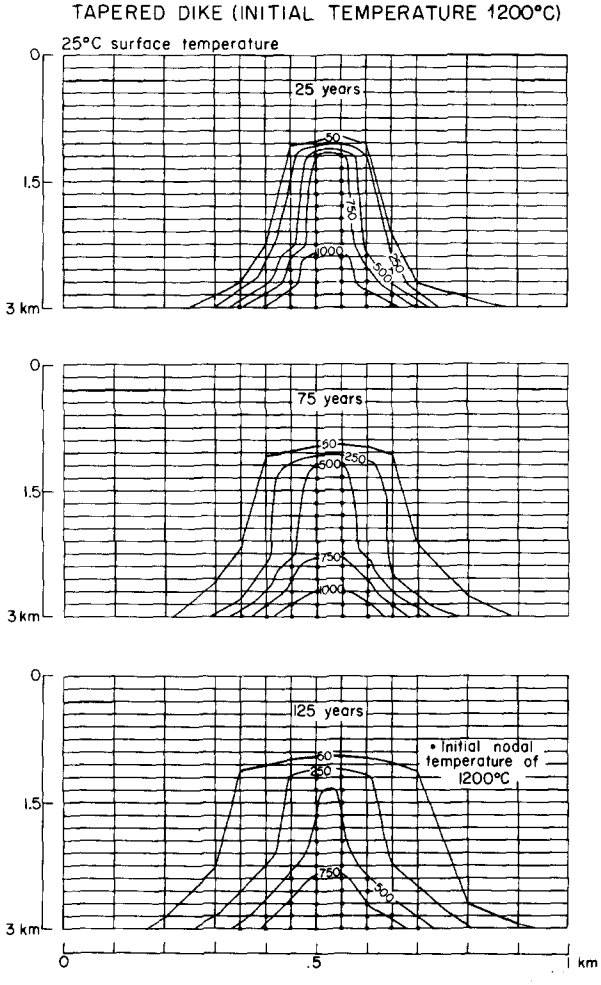

Fig. 8. Isotherms around an initial temperature distribution of 1200°C (at dots). The dots construct a tapered dike that is 50 m wide for the upper 1200 m. Isotherms are at 25, 75, and 125 years after application of the initial temperatures.

In this model a dike is simulated by setting initial temperatures of 1200° C at the nodes indicates by dots (Fig. 8). The dots define a vertical dike, 1200 m high, 50 m wide, with top 1.2 km below the surface. The dike thickens to 150 m at a depth of 2.4 km and tapers to its maximum width of 350 m at 3 km depth. Computer plots show the flow of heat at 25, 75, and 125 years (Fig. 8). The material in the dike is observed to cool as the surrounding region is heated. Plots of HGP-A temperatures and model temperatures 75 and 125 m from the dike center show fair correlation at 125 years (Fig. 9) and is considered to be the best fit of the three models studied. The minor oscillations on the model data are attributed to approximations in the finite element size. A change in the horizontal dimension of the element size from 1.0 km to 0.25 km decreased the oscillations. Changes in time steps from one to twenty-five years did not, however, significantly influence the results. Changes in diffusivity have a direct linear effect on time.

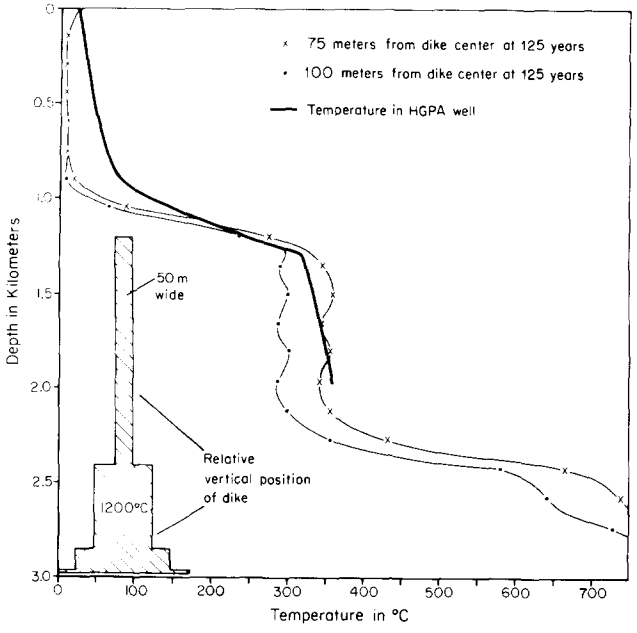

Fig. 9. Plot of observed temperatures in the HGP-A well and temperatures at 75 and 100 m from the dike center 125 years after injection.

CONCLUSIONS

The models presented above show that a reasonable approximation to the temperature distribution in the lower part of HGP-A could result from heat conduction from a tapered dike complex as approximated by Model III. Our model studies suggest that the dike complex is 50 m thick in the upper 1200 m, and then increased in thickness to 350 m at a depth of about 3 km.

A more realistic model would be a series of thin dikes repeatedly injected along the same fissures. As each new dike is injected, previously heated materials would be forced apart and the model would be in effect a combination of mass transport and conduction. We are presently modifying our program to accomodate such a model. For this study, however, we have assumed that the thin dikes have coalesced into one unit (50 m or more in thickness), and we have examined the temperature distribution at time intervals of 25 to 125 years after injection. This provides a first approximation from which to evaluate the necessity of more complex models.

Palmiter (1976) and Stone (1977) report that the degree of alteration and the degree of filling of fractures and vesicules increase in the lower part of HGP-A, and that filling is nearly complete below about 1.3 km. This data implies that while some movement of fluids has occurred in the past, the overall permeability decreases with time, and that at the present time convection may be very restricted below 1.3 km in the rift zone. Perhaps under normal conditions convection is so slow that conduction heat transport has a significant effect in establishing the overall temperature distribution in the ERZ. Removing large quantities of water from HGP-A will obviously increase the convective component in the nearby section of the ERZ; however, the conduction component must be considered in evaluating the energy potential of the HGP-A reservoir.

ACKNOWLEDGEMENTS

This study was supported by the Direct Heat Resource Assessment Project funded by the Department of Energy (DE-AC03-80SF-10819). Charles Helsley initially suggested the study and Jim Kauahikaua critically read the manuscript and many of his suggestions have been incorporated into the text.

REFERENCES

Blevins, J.Y.K., Jr., 1981. Subsidence Mechanics of Kilauean Pit Craters. M. S. Thesis, Univ. of Hawaii, 108 pp.

Bullard, E.C., 1947. The time necessary for a bore hole to attain temperature equilibrium. Mon. Not. R. Astron. Soc., Geophys. Sup., 5: 127—130.

Cheng, P. and Lau, K.H., 1978. Modelling of a Volcanic Island Geothermal Reservoir. Hawaii Geothermal Project Report, College of Engineering, University of Hawaii, 39 pp.

Dzurisin, D., Anderson, L.A., Eaton, G.P., Koyanagi, R.Y., Lipman, P.W., Lockwood, J.P., Okamura, R.T., Puniwai, G.S., Sako, M.K. and Yamashita, K.M., 1980. Geophysical observations of Kilauea volcano, Hawaii, 2. Constraints of the magma supply during November 1975—September 1977, J. Volcanol. Geothermal Res., 7: 241—269.

Eaton, J.P., 1962. Crustal structure and volcanism in Hawaii. In: G.A. Macdonald and H. Kuro (Editors), The Crust of the Pacific Basin. Am. Geophys. Union, Geophys. Monogr. Ser., 6: 13—29.

Eaton, J.P. and Murata, K.J., 1960. How volcanoes grow. Science, 132: 925—938.

Epp, D., Decker, R.W. and Okamura, A.T., 1983. Relation of summit deformation to East Rift Zone eruptions on Kilauea volcano, Hawaii. Geophys. Res. Lett., in press.

Fiske, K.S. and Kinoshita, W.T., 1969. Inflation of Kilauea volcano prior to the 1967—1968 eruption. Science, 165: 341—349.

Helsley, C.E., 1977. Geothermal potential for Hawaii in light of HGP-A. Geotherm. Res. Council, Trans., 1: 137—138.

Horai, K.I., 1974. Heat flow anomaly associated with dike intrusion, 1. J. Geophys. Res., 79: 1640—1646.

Klein, F.W., 1982. Patterns of historical eruptions at Hawaiian volcanoes. J. Volcanol. Geothermal Res., 12: 1—35.

Koyanagi, R.Y., Endo, E.T. and Ward, P.L., 1976. Seismic activity on the Island of Hawaii, 1970 to 1973. In: G.H. Sutton, M.H. Manghnani and R. Moberly (Editors), Geophysics of the Pacific Basin and its Margin. Am. Geophys. Union, Geophys. Monogr. Ser., 19: 169—172.

Lachenbruch, A.H. and Brewer, M.C., 1959. Dissipation of the temperature effect of drilling a well in arctic Alaska. U.S. Geol. Surv. Bull., 1083-C: 73—109.

Lee, T.C., Rudman, A.J. and Sjoreen, A., 1980. Application of Finite-Element Analysis to Terrestrial Heat Flow. Indiana, Geol. Surv. Occasional Paper 29, 53 pp.

Macdonald, G.A., 1977. Geology and ground-water hydrology. In: A.S. Furumoto, G.A. Macdonald, M. Druecker and P.-F. Fan (Editors), Preliminary Studies for Geothermal Exploration in Hawaii, 1973—1975. Report HIG-75-5, Hawaii Inst. Geophys, 55 pp.

Macdonald, G.A. and Eaton, J.P., 1964. Hawaiian Volcanoes during 1955. U. S. Geol. Surv. Bull., 1171: 170.

Manghnani, M.H., Rai, C.S. and Hamada, T., 1976. Physical properties of rocks. Hawaii Geothermal Project, Initial Phase II Progress Report, Feb.

Manghnani, M.H., Rai, C.S. and Hamada, T., 1977. Physical properties of rocks. Hawaii Geothermal Project, Phase III Progress Report, Jan.

Palmiter, D.B., 1976. Geology of HGP-A from macroscopic study of cores and cuttings. (unpubl.).

Robertson, E.C. and Peck, D.L., 1974. Thermal conductivity of vesicular basalt from Hawaii. J. Geophys. Res., 79: 4875—4888.

Swanson, D.A., 1972. Magma supply rate of Kilauea volcano 1952—1971. Science, 175: 169—170.

Stone, C., 1977. Chemistry, Petrography, and Hydrothermal Alteration of Basalts from Hawaii Geothermal Project Well-A, Kilauea, Hawaii. M.S. Thesis, Univ. of Hawaii, 84 pp.

Suyenaga, W. and Furumoto, A.S., 1978. Microearthquake study of the East Rift Zone of Kilauea, Puna, Hawaii. In: Seismic Studies of Kilauea Volcano, Hawaii Island. Hawaii Inst. Geophys. Tech. Rept. HIG-78-8.

Wright, T.L. and Fiske, R.S., 1971. Origin of the differentated and hybrid lavas of Kilauea volcano, Hawaii. J. Petrol., 12: 1—65.

Zablocki, C.J. and Koyanagi, R.Y., 1979. An anomalous structure in the lower East Rift Zone of Kilauea volcano, Hawaii, inferred from geophysical data. In: Abstract Volume, Hawaii Symposium on Intraplate Volcanism and Submarine Volcanism. Hilo, Hawaii, p. 177.

Zienkiewicz, C.O., 1977. The Finite Element Method. McGraw-Hill, New York, N.Y., 787 pp.